Advances in Applied Mathematics and Mechanics
Adv. Appl. Math. Mech., Vol. **3**, No. 6, pp. 663-688

DOI: 10.4208/aamm.11-m1183
December 2011

Multi-Symplectic Wavelet Collocation Method for Maxwell's Equations

Huajun Zhu*, Songhe Song and Yaming Chen

Department of Mathematics and System Science, School of Science, National University of Defense Technology, Changsha 410073, China

Received 30 April 2011; Accepted (in revised version) 7 May 2011
Available online 31 October 2011

Abstract. In this paper, we develop a multi-symplectic wavelet collocation method for three-dimensional (3-D) Maxwell's equations. For the multi-symplectic formulation of the equations, wavelet collocation method based on autocorrelation functions is applied for spatial discretization and appropriate symplectic scheme is employed for time integration. Theoretical analysis shows that the proposed method is multi-symplectic, unconditionally stable and energy-preserving under periodic boundary conditions. The numerical dispersion relation is investigated. Combined with splitting scheme, an explicit splitting symplectic wavelet collocation method is also constructed. Numerical experiments illustrate that the proposed methods are efficient, have high spatial accuracy and can preserve energy conservation laws exactly.

AMS subject classifications: 37M15, 65P10, 65M70, 65T60

Key words: Multi-symplectic, wavelet collocation method, Maxwell's equations, symplectic, conservation laws.

1 Introduction

Maxwell's equations are the most foundational equations in electromagnetism and play an important role in a large number of engineering applications. It is of much significance to develop effective numerical methods to simulate Maxwell's equations with two or three spatial dimensions. Nowadays, a great deal of numerical methods have been used to solve the Maxwell's equations. The finite-difference time-domain (FDTD) method for the one-dimensional Maxwell's equations was first proposed by Yee in [1], which is simple and flexible but is conditionally stable. The FDTD requires large memory and CPU time to obtain accurate solutions for high-dimensional problem. Thus, the FDTD is not a computationally efficient method. Actually, the intensive memory and CPU time requirements mainly come from two aspects: small

*Corresponding author.
Email: girl-zhu@163.com (H. Zhu), shsong@nudt.edu.cn (S. Song), chenym-08@163.com (Y. Chen)

spatial step because of low spatial accuracy and small time step because of stability constraints. For the first pitfall, Krumpholz and Katehi developed a multiresolution time-domain (MRTD) method [2], which has high spatial accuracy but has stringent stability constraints. For the second constraints, some unconditionally stable methods were also constructed. Zheng et al. proposed an ADI-FDTD method for the 3-D Maxwell's equations with an isotropic and lossless medium in [3], but they had't made simulations. Combining splitting method with FDTD scheme, Gao et al. constructed a splitting FDTD method for the 2-D Maxwell's equations and applied the method to solve a scattering problem successfully [4].

On the other hand, during modern numerical simulation procedure, it is significant to construct numerical methods to preserve the intrinsic properties of the original system, such methods are called structure preserving methods containing energy-preserving methods, symplectic methods, multi-symplectic methods, and so on. The ADI-FDTD and splitting FDTD methods may break the energy conservation property of the Maxwell's equations. To overcome the problem, symplectic FDTD scheme [5], which is conditionally stable, energy-conserved splitting FDTD methods [6] and discontinuous Hamiltonian finite element methods [7] were developed. Recently, multi-symplectic algorithms are developed rapidly for multi-symplectic Hamiltonian PDEs due to their long-term behavior and good preservation of local conservation laws [8–19]. However, multi-symplectic schemes are seldom considered for the Maxwell's equations. A new multi-symplectic self-adjoint scheme was developed to simulate the 2-D Maxwell's equations in [20], which is difficult to be applied for 3-D problems. Kong et al. proposed splitting multi-symplectic integrators for Maxwell's equations [22], where the central box scheme was used to discrete the sub-Hamiltonian systems. The 3-D Maxwell's equations were well simulated and good energy-preserving properties were also obtained. However, the convergence rate of the methods is not high. To construct a numerical method which is unconditionally stable and energy-preserving and has high accuracy motivates the current work.

Recently, we have proposed symplectic wavelet collocation method (SWCM) and multi-symplectic wavelet collocation method (MSWCM) for Hamiltonian PDEs in [23, 24]. These methods have the merits of high accuracy, less computations, singularity capturing, invariants preserving properties, and have been applied for solving 2-D Schrödinger equations in [25]. In this paper, we generalize the MSWCM to solve the 3-D Maxwell's equations. The method can obtain expected numerical errors with much less grid points because of high spatial accuracy and takes less computations because of sparse spatial differentiation matrices. We prove that the MSWCM is unconditionally stable and can preserve the two energy conservation laws of the Maxwell's equations exactly under periodic boundary conditions. The dispersion relation for the MSWCM is also investigated. In addition, the properties of the wavelet spectral matrix are analyzed in detail. Then an explicit splitting symplectic wavelet collocation method (ES-SWCM) is also constructed and compared with the MSWCM. Moreover, numerical simulations for the 2-D and 3-D Maxwell's equations are taken and a deep numerical investigation showing the tradeoff between computational effort and error

is made. Furthermore, the MSWCM is compared with other methods, such as the discontinuous Hamiltonian finite element methods and the splitting multi-symplectic methods.

The rest of this paper is organized as follows. In Section 2, the MSWCM is proposed for the 3-D Maxwell's equations and proved to have discrete multi-symplectic conservation laws. In Section 3, stability and energy-preserving properties of the MSWCM are analyzed. The ES-SWCM is constructed in Section 4. In Section 5, numerical experiments for the 2-D and 3-D Maxwell's equations are presented. Moreover, comparisons with other methods are also made. Finally, concluding remarks are given in Section 6.

2 MSWCM for the 3-D Maxwell's equations

In this section, we briefly introduce the multi-symplectic formulation and conservation laws of 3-D Maxwell's equations, then we propose the MSWCM for the 3-D Maxwell's equations and prove that the proposed method is multi-symplectic.

2.1 Multi-symplectic formulation of the 3-D Maxwell's equations

For a linear homogeneous medium with permittivity ε and permeability μ, the 3-D Maxwell's equations with no charges and currents can be written in curl equations

$$\begin{cases} \dfrac{\partial \mathbf{E}}{\partial t} = \dfrac{1}{\varepsilon}\nabla \times \mathbf{H}, \\ \dfrac{\partial \mathbf{H}}{\partial t} = -\dfrac{1}{\mu}\nabla \times \mathbf{E}, \end{cases} \tag{2.1}$$

where $\mathbf{E}= (E_x, E_y, E_z)^{\mathrm{T}}$ is the electric field and $\mathbf{H} = (H_x, H_y, H_z)^{\mathrm{T}}$ is the magnetic field. The curl equations (2.1) can be split into six scalar equations [6,22]

$$\begin{cases} \dfrac{\partial E_x}{\partial t} = \dfrac{1}{\varepsilon}\Big(\dfrac{\partial}{\partial y}H_z - \dfrac{\partial}{\partial z}H_y\Big), \\ \dfrac{\partial E_y}{\partial t} = \dfrac{1}{\varepsilon}\Big(\dfrac{\partial}{\partial z}H_x - \dfrac{\partial}{\partial x}H_z\Big), \\ \dfrac{\partial E_z}{\partial t} = \dfrac{1}{\varepsilon}\Big(\dfrac{\partial}{\partial x}H_y - \dfrac{\partial}{\partial y}H_x\Big), \\ \dfrac{\partial H_x}{\partial t} = -\dfrac{1}{\mu}\Big(\dfrac{\partial}{\partial y}E_z - \dfrac{\partial}{\partial z}E_y\Big), \\ \dfrac{\partial H_y}{\partial t} = -\dfrac{1}{\mu}\Big(\dfrac{\partial}{\partial z}E_x - \dfrac{\partial}{\partial x}E_z\Big), \\ \dfrac{\partial H_z}{\partial t} = -\dfrac{1}{\mu}\Big(\dfrac{\partial}{\partial x}E_y - \dfrac{\partial}{\partial y}E_x\Big). \end{cases} \tag{2.2}$$

Let

$$\mathbf{z} = (\mathbf{H_x}, \mathbf{H_y}, \mathbf{H_z}, \mathbf{E_x}, \mathbf{E_y}, \mathbf{E_z})^{\mathrm{T}},$$

Eq. (2.2) can be written as a multi-symplectic PDE

$$M\mathbf{z}_t + K_1\mathbf{z}_x + K_2\mathbf{z}_y + K_3\mathbf{z}_z = \nabla_{\mathbf{z}} S(\mathbf{z}), \tag{2.3}$$

with $S(\mathbf{z}) = 0$ and the skew-symmetric matrices

$$M = \begin{bmatrix} 0 & 0 & 0 & 1 & 0 & 0 \\ 0 & 0 & 0 & 0 & 1 & 0 \\ 0 & 0 & 0 & 0 & 0 & 1 \\ -1 & 0 & 0 & 0 & 0 & 0 \\ 0 & -1 & 0 & 0 & 0 & 0 \\ 0 & 0 & -1 & 0 & 0 & 0 \end{bmatrix}, \qquad K_1 = \begin{bmatrix} 0 & 0 & 0 & 0 & 0 & 0 \\ 0 & 0 & -\frac{1}{\varepsilon} & 0 & 0 & 0 \\ 0 & \frac{1}{\varepsilon} & 0 & 0 & 0 & 0 \\ 0 & 0 & 0 & 0 & 0 & 0 \\ 0 & 0 & 0 & 0 & 0 & -\frac{1}{\mu} \\ 0 & 0 & 0 & 0 & \frac{1}{\mu} & 0 \end{bmatrix},$$

$$K_2 = \begin{bmatrix} 0 & 0 & \frac{1}{\varepsilon} & 0 & 0 & 0 \\ 0 & 0 & 0 & 0 & 0 & 0 \\ -\frac{1}{\varepsilon} & 0 & 0 & 0 & 0 & 0 \\ 0 & 0 & 0 & 0 & 0 & \frac{1}{\mu} \\ 0 & 0 & 0 & 0 & 0 & 0 \\ 0 & 0 & 0 & -\frac{1}{\mu} & 0 & 0 \end{bmatrix}, \qquad K_3 = \begin{bmatrix} 0 & -\frac{1}{\varepsilon} & 0 & 0 & 0 & 0 \\ \frac{1}{\varepsilon} & 0 & 0 & 0 & 0 & 0 \\ 0 & 0 & 0 & 0 & 0 & 0 \\ 0 & 0 & 0 & 0 & -\frac{1}{\mu} & 0 \\ 0 & 0 & 0 & \frac{1}{\mu} & 0 & 0 \\ 0 & 0 & 0 & 0 & 0 & 0 \end{bmatrix}.$$

The multi-symplectic system (2.3) has a multi-symplectic conservation law [9]

$$\frac{\partial}{\partial t}\omega + \frac{\partial}{\partial x}\kappa_x + \frac{\partial}{\partial y}\kappa_y + \frac{\partial}{\partial z}\kappa_z = 0, \tag{2.4}$$

with the differential 2-forms

$$\omega = d\mathbf{z} \wedge M d\mathbf{z}, \quad \kappa_x = d\mathbf{z} \wedge K_1 d\mathbf{z}, \quad \kappa_y = d\mathbf{z} \wedge K_2 d\mathbf{z}, \quad \kappa_z = d\mathbf{z} \wedge K_3 d\mathbf{z}.$$

Under the perfectly electric conducting boundary condition, the Maxwell's equations (2.1) can be proved to have the following two energy conservation laws

$$\text{Energy I}: \qquad \int_\Omega \left(\varepsilon|\mathbf{E}(x,t)|^2 + \mu|\mathbf{H}(x,t)|^2\right) d\Omega = C_1, \tag{2.5a}$$

$$\text{Energy II}: \qquad \int_\Omega \left(\varepsilon\left|\frac{\partial \mathbf{E}(x,t)}{\partial t}\right|^2 + \mu\left|\frac{\partial \mathbf{H}(x,t)}{\partial t}\right|^2\right) d\Omega = C_2, \tag{2.5b}$$

where C_1 and C_2 are constants. For more details, see [6, 22].

In this paper, we consider periodic boundary conditions on the cubic spatial domain

$$\Omega = [x_L, x_R] \times [y_L, y_R] \times [y_L, y_R].$$

Firstly, by Green formula, we have

$$\frac{\partial\langle\varepsilon\mathbf{E},\mathbf{E}\rangle}{\partial t}+\frac{\partial\langle\mu\mathbf{H},\mathbf{H}\rangle}{\partial t}=\langle\nabla\times\mathbf{E},\mathbf{H}\rangle-\langle\nabla\times\mathbf{H},\mathbf{E}\rangle$$
$$=\int_\Omega\nabla\cdot(\mathbf{E}\times\mathbf{H})d\Omega=\int_{\partial\Omega}(\mathbf{E}\times\mathbf{H})\cdot\mathbf{n}dS.$$

Second, under the periodic boundary conditions, we have

$$\mathbf{E}^L=\mathbf{E}^R,\qquad\mathbf{H}^L=\mathbf{H}^R,\qquad\mathbf{n}^L=-\mathbf{n}^R,$$

so it can be easily observed that

$$\int_{\partial\Omega}(\mathbf{E}\times\mathbf{H})\cdot\mathbf{n}dS=0.$$

Thus, the Maxwell's equations (2.1) have the first energy conservation law (2.5a). Similarly, since

$$\Big(\frac{\partial\mathbf{E}}{\partial t}\Big)^L=\Big(\frac{\partial\mathbf{E}}{\partial t}\Big)^R,\qquad\Big(\frac{\partial\mathbf{H}}{\partial t}\Big)^L=\Big(\frac{\partial\mathbf{H}}{\partial t}\Big)^R,\qquad\mathbf{n}^L=-\mathbf{n}^R,$$

we have

$$\int_{\partial\Omega}\Big(\frac{\partial\mathbf{E}}{\partial t}\times\frac{\partial\mathbf{H}}{\partial t}\Big)\cdot\mathbf{n}dS=0.$$

So the Maxwell's equations (2.1) also have the second energy conservation law (2.5b).

In the 2-D transverse magnetic (TM) polarization case, the electric field is $\mathbf{E}=(0,0,E_z)^{\mathrm{T}}$ and the magnetic field is $\mathbf{H}=(H_x,H_y,0)^{\mathrm{T}}$. Therefore, the 2-D Maxwell's equations read

$$\begin{cases}\dfrac{\partial E_z}{\partial t}=\dfrac{1}{\varepsilon}\Big(\dfrac{\partial H_y}{\partial x}-\dfrac{\partial H_x}{\partial y}\Big),\\[2mm]\dfrac{\partial H_x}{\partial t}=-\dfrac{1}{\mu}\dfrac{\partial E_z}{\partial y},\\[2mm]\dfrac{\partial H_y}{\partial t}=\dfrac{1}{\mu}\dfrac{\partial E_z}{\partial x}.\end{cases}\tag{2.6}$$

In the 2-D transverse electric (TE) polarization case, the electric field is $\mathbf{E}=(E_x,E_y,0)^{\mathrm{T}}$ and the magnetic field is $\mathbf{H}=(0,0,H_z)^{\mathrm{T}}$. Therefore, the 2-D Maxwell's equations become

$$\begin{cases}\dfrac{\partial E_x}{\partial t}=\dfrac{1}{\varepsilon}\dfrac{\partial H_z}{\partial y},\\[2mm]\dfrac{\partial E_y}{\partial t}=-\dfrac{1}{\varepsilon}\dfrac{\partial H_z}{\partial x},\\[2mm]\dfrac{\partial H_z}{\partial t}=\dfrac{1}{\mu}\Big(\dfrac{\partial E_x}{\partial y}-\dfrac{\partial E_y}{\partial x}\Big).\end{cases}\tag{2.7}$$

2.2 MSWCM for the 3-D Maxwell's equations

Based on autocorrelation functions $\theta(x)$ of Daubechies scaling function, the SWCM and MSWCM have been proposed for 1-D Hamiltonian PDEs in [23, 24]. Consider periodic boundary conditions in $[0, L]$ (L is an integer) and a fixed scale J = constant (with grid points $N = L \cdot 2^J$), the differentiation matrix B_1 for the first-order partial differential operator ∂x is an $N \times N$ sparse anti-symmetric circulant matrix:

$$B_1 = 2^J \cdot Circ\big(\theta'(0), \theta'(-1), \cdots, \theta'(-(M-1)), 0, \cdots, 0, \theta'(M-1), \cdots, \theta'(1)\big),$$

where M is the order of Daubechies scaling function. Here $\theta'(l)$, $(l = -(M-1), \cdots, (M-1))$ are the values of the function $\theta'(x)$ at integer points, which can be obtained numerically. See [23, 24, 26–28] for more details.

Now, we construct a MSWCM for the 3-D Maxwell's equations (2.2) using the wavelet collocation method in [23, 24]. Consider periodic boundary conditions with $N_x \times N_y \times N_z$ grid points, where

$$N_x = L_x \cdot 2^{J_x}, \qquad N_y = L_y \cdot 2^{J_y}, \qquad N_z = L_z \cdot 2^{J_z}.$$

Take E_x for example, we can approximate $E_x(x, y, z, t)$ by interpolation operator $IE_x(x, y, z, t)$, which interpolates $E_x(x, y, z, t)$ at collocation points

$$(x_l, y_j, z_k) = \Big(\frac{l}{2^{J_x}}, \frac{j}{2^{J_y}}, \frac{k}{2^{J_z}}\Big),$$

for $l = 1, \cdots, N_x$, $j = 1, \cdots, N_y$, $k = 1, \cdots, N_z$,

$$IE_x(x, y, z, t) = \sum_{l=1}^{N_x} \sum_{j=1}^{N_y} \sum_{k=1}^{N_z} E_{x_{l,j,k}} \theta\big(2^{J_x} x - l\big) \theta\big(2^{J_y} y - j\big) \theta\big(2^{J_z} z - k\big). \tag{2.8}$$

We substitute the interpolation operators into the multi-symplectic Hamiltonian PDEs (2.2), and require that (2.2) is satisfied exactly at collocation points. The crucial step is to obtain values for the derivatives in (2.2). Making partial differential in the y-direction with (2.8) and evaluating the resulting expressions at collocation points, we obtain

$$\begin{aligned}
\frac{\partial IE_x(x_l, y_j, z_k, t)}{\partial y} &= \sum_{l'=1}^{N_x} \sum_{j'=1}^{N_y} \sum_{k'=1}^{N_z} E_{x_{l',j',k'}} \theta(2^{J_x} x_l - l') \theta(2^{J_z} z_k - k') \frac{\theta(2^{J_y} y - j')}{dy}\Big|_{y_j} \\
&= \sum_{j'=1}^{N} E_{x_{l,j',k}} \big(2^{J_y} \theta'(j - j')\big) = \sum_{j'=j-(M-1)}^{j+(M-1)} E_{x_{l,j',k}} (B_1^y)_{j,j'} \\
&= \big((I_{N_x} \otimes B_1^y \otimes I_{N_z}) \mathbf{E_x}\big)_{l,j,k},
\end{aligned} \tag{2.9}$$

where $\otimes$ means Kronecker inner product, I_{N_x} is the $N_x \times N_x$ identity matrix, B_1^y is the $N_y \times N_y$ first-order differentiation matrix in the y-direction,

$$\begin{aligned}
\mathbf{E_x}^n = \Big(& E_{x_{1,1,1}}^n, E_{x_{2,1,1}}^n, \cdots, E_{x_{Nx,1,1}}^n, \cdots, E_{x_{1,Ny,1}}^n, E_{x_{2,Ny,1}}^n, \cdots, \\
& E_{x_{Nx,Ny,1}}^n, \cdots, E_{x_{1,Ny,Nz}}^n, E_{x_{2,Ny,Nz}}^n, \cdots, E_{x_{Nx,Ny,Nz}}^n \Big)^{\mathrm{T}},
\end{aligned}$$

etc.

Combining with the first-order differentiation matrices, we apply the wavelet collocation method to discrete the multi-symplectic Hamiltonian PDEs (2.2) in space, and then integrate the semi-discrete system by symplectic scheme the implicit midpoint rule in time. We obtain a MSWCM for the 3-D Maxwell's equations (2.2)

$$\begin{cases} \dfrac{\mathbf{E_x}^{n+1}-\mathbf{E_x}^{n}}{\tau}=\dfrac{1}{\varepsilon}(A_2\mathbf{H_z}^{n+\frac{1}{2}}-A_3\mathbf{H_y}^{n+\frac{1}{2}}),\\ \dfrac{\mathbf{E_y}^{n+1}-\mathbf{E_y}^{n}}{\tau}=\dfrac{1}{\varepsilon}(A_3\mathbf{H_x}^{n+\frac{1}{2}}-A_1\mathbf{H_z}^{n+\frac{1}{2}}),\\ \dfrac{\mathbf{E_z}^{n+1}-\mathbf{E_z}^{n}}{\tau}=\dfrac{1}{\varepsilon}(A_1\mathbf{H_y}^{n+\frac{1}{2}}-A_2\mathbf{H_x}^{n+\frac{1}{2}}),\\ \dfrac{\mathbf{H_x}^{n+1}-\mathbf{H_x}^{n}}{\tau}=-\dfrac{1}{\mu}(A_2\mathbf{E_z}^{n+\frac{1}{2}}-A_3\mathbf{E_y}^{n+\frac{1}{2}}),\\ \dfrac{\mathbf{H_y}^{n+1}-\mathbf{H_y}^{n}}{\tau}=-\dfrac{1}{\mu}(A_3\mathbf{E_x}^{n+\frac{1}{2}}-A_1\mathbf{E_z}^{n+\frac{1}{2}}),\\ \dfrac{\mathbf{H_z}^{n+1}-\mathbf{H_z}^{n}}{\tau}=-\dfrac{1}{\mu}(A_1\mathbf{E_y}^{n+\frac{1}{2}}-A_2\mathbf{E_x}^{n+\frac{1}{2}}), \end{cases} \tag{2.10}$$

where τ is the time-step,

$$\mathbf{E_x}^{n+\frac{1}{2}}=\frac{1}{2}(\mathbf{E_x}^{n+1}+\mathbf{E_x}^{n}) \quad \text{and} \quad \mathbf{E_y}^{n+\frac{1}{2}}=\frac{1}{2}(\mathbf{E_y}^{n+1}+\mathbf{E_y}^{n}),$$

etc. Here

$$A_1=(B_1^x\otimes I_{N_y}\otimes I_{N_z}),\quad A_2=(I_{N_x}\otimes B_1^y\otimes I_{N_z}),\quad A_3=(I_{N_x}\otimes I_{N_y}\otimes B_1^z),$$

which are all anti-symmetric matrices. Although the MSWCM (2.10) is an implicit scheme, the spatial differentiation matrices are sparse and direct fixed-point iteration method can be used in solving, which renders the proposed MSWCM much efficient.

The MSWCM (2.10) can be rewritten as

$$\begin{aligned} M\frac{\mathbf{z}_{l,j,k}^{n+1}-\mathbf{z}_{l,j,k}^{n}}{\tau}&+\sum_{l'=l-(M-1)}^{l+(M-1)}(B_1^x)_{l,l'}\big(K_1\mathbf{z}_{l',j,k}^{n+\frac{1}{2}}\big)+\sum_{j'=j-(M-1)}^{j+(M-1)}(B_1^y)_{j,j'}\big(K_2\mathbf{z}_{l,j',k}^{n+\frac{1}{2}}\big)\\ &+\sum_{k'=k-(M-1)}^{k+(M-1)}(B_1^z)_{k,k'}\big(K_3\mathbf{z}_{l,j,k'}^{n+\frac{1}{2}}\big)=0, \end{aligned} \tag{2.11}$$

which is equivalent to the following compact form

$$M\frac{\mathbf{Z}^{n+1}-\mathbf{Z}^{n}}{\tau}+A_1\otimes K_1\mathbf{Z}^{n+\frac{1}{2}}+A_2\otimes K_2\mathbf{Z}^{n+\frac{1}{2}}+A_3\otimes K_3\mathbf{Z}^{n+\frac{1}{2}}=0, \tag{2.12}$$

where

$$\mathbf{Z}^{n}=\big((\mathbf{H_x}^{n})^{\mathrm{T}},(\mathbf{H_y}^{n})^{\mathrm{T}},(\mathbf{H_z}^{n})^{\mathrm{T}},(\mathbf{E_x}^{n})^{\mathrm{T}},(\mathbf{E_y}^{n})^{\mathrm{T}},(\mathbf{E_z}^{n})^{\mathrm{T}}\big)^{\mathrm{T}}.$$

Theorem 2.1. *The MSWCM* (2.11) *has the following discrete multi-symplectic conservation laws*

$$\frac{\omega^{n+1}_{l,j,k}-\omega^{n}_{l,j,k}}{\tau}+\sum_{l'=l-(M-1)}^{l+(M-1)}(B^{x}_{1})_{l,l'}\kappa^{n+\frac{1}{2}}_{x_{l',l,j,k}}+\sum_{j'=j-(M-1)}^{j+(M-1)}(B^{y}_{1})_{j,j'}\kappa^{n+\frac{1}{2}}_{y_{j',l,j,k}}+\sum_{k'=k-(M-1)}^{z+(M-1)}(B^{z}_{1})_{k,k'}\kappa^{n+\frac{1}{2}}_{z_{k',l,j,k}}=0, \tag{2.13}$$

where

$$\omega^{n}_{l,j,k}=\frac{1}{2}d\mathbf{z}^{n}_{l,j,k}\wedge Md\mathbf{z}^{n}_{l,j,k},\qquad \kappa^{n+\frac{1}{2}}_{x_{l',l,j,k}}=d\mathbf{z}^{n+\frac{1}{2}}_{l,j,k}\wedge K_1 d\mathbf{z}^{n+\frac{1}{2}}_{l',j,k},$$
$$\kappa^{n+\frac{1}{2}}_{y_{j',l,j,k}}=d\mathbf{z}^{n+\frac{1}{2}}_{l,j,k}\wedge K_2 d\mathbf{z}^{n+\frac{1}{2}}_{l,j',k},\qquad \kappa^{n+\frac{1}{2}}_{z_{k',l,j,k}}=d\mathbf{z}^{n+\frac{1}{2}}_{l,j,k}\wedge K_3 d\mathbf{z}^{n+\frac{1}{2}}_{l,j,k'}.$$

Proof. The corresponding variational equation of (2.11) is

$$M\frac{d\mathbf{z}^{n+1}_{l,j,k}-d\mathbf{z}^{n}_{l,j,k}}{\tau}+\sum_{l'=l-(M-1)}^{l+(M-1)}(B^{x}_{1})_{l,l'}\left(K_1 d\mathbf{z}^{n+\frac{1}{2}}_{l',j,k}\right)+\sum_{j'=j-(M-1)}^{j+(M-1)}(B^{y}_{1})_{j,j'}\left(K_2 d\mathbf{z}^{n+\frac{1}{2}}_{l,j',k}\right)+\sum_{k'=k-(M-1)}^{k+(M-1)}(B^{z}_{1})_{k,k'}\left(K_3 d\mathbf{z}^{n+\frac{1}{2}}_{l,j,k'}\right)=0. \tag{2.14}$$

Taking the wedge product with $d\mathbf{z}^{n+1/2}_{l,j,k}$ on both sides of (2.14), we can obtain the multi-symplectic conservation laws (2.13). We briefly denote the MSWCM with ADM as MSM. □

3 Stability, dispersion and energy-preserving property

In this section, we will prove that the proposed MSWCM is unconditionally stable and conserves the two energy conservation laws (2.5a) and (2.5b) exactly.

Theorem 3.1. *Under periodic boundary conditions, the MSWCM* (2.10) *is unconditionally stable.*

Proof. Let h_x, h_y, h_z be the spatial steps in the x, y, z directions respectively, J_x, J_y, J_z and N_x, N_y, N_z are corresponding scales and grid numbers. Set

$$\begin{bmatrix}\mathbf{E}^{n}_{l,j,k}\\ \mathbf{H}^{n}_{l,j,k}\end{bmatrix}=\begin{bmatrix}\mathbf{E}\\ \mathbf{H}\end{bmatrix}^{n}e^{i(k_x l h_x+k_y j h_y+k_z k h_z)}, \tag{3.1}$$

where

$$\mathbf{E}^{n}_{l,j,k}=(E_{x}{}^{n}_{l,j,k},E_{y}{}^{n}_{l,j,k},E_{z}{}^{n}_{l,j,k})^{\mathrm{T}}\quad\text{and}\quad\mathbf{H}^{n}_{l,j,k}=(H_{x}{}^{n}_{l,j,k},H_{y}{}^{n}_{l,j,k},H_{z}{}^{n}_{l,j,k})^{\mathrm{T}}.$$

Substituting (3.1) into the scheme (2.10), we obtain

$$\begin{bmatrix} I_{3\times3} & c_1D \\ -c_2D & I_{3\times3} \end{bmatrix} \begin{bmatrix} \mathbf{E} \\ \mathbf{H} \end{bmatrix}^{n+1} = \begin{bmatrix} I_{3\times3} & -c_1D \\ c_2D & I_{3\times3} \end{bmatrix} \begin{bmatrix} \mathbf{E} \\ \mathbf{H} \end{bmatrix}^{n}, \tag{3.2}$$

where

$$c_1 = \frac{\tau}{2\varepsilon}, \qquad c_2 = \frac{\tau}{2\mu}, \qquad D = \begin{bmatrix} 0 & d_3 & -d_2 \\ -d_3 & 0 & d_1 \\ d_2 & -d_1 & 0 \end{bmatrix},$$

$$d_1 = 2^{J_x} \sum_{l=-(M-1)}^{M-1} e^{-ik_x lh_x}\theta'(-l) = 2^{J_x}\Big(\theta'(0) + \sum_{l=1}^{M-1} e^{ik_x lh_x}\theta'(l) + \sum_{l=1}^{M-1} e^{-ik_x lh_x}\theta'(-l)\Big)$$

$$= 2^{J_x}\Big(\theta'(0) + \sum_{l=1}^{M-1} \theta'(l)(e^{ik_x lh_x} - e^{-ik_x lh_x})\Big) = i2^{J_x} \sum_{l=1}^{M-1} 2\theta'(l)\sin(k_x lh_x).$$

Similarly,

$$d_2 = i2^{J_y} \sum_{j=1}^{M-1} 2\theta'(j)\sin(k_y jh_y), \qquad d_3 = i2^{J_z} \sum_{k=1}^{M-1} 2\theta'(k)\sin(k_z kh_z).$$

It is easy to know that d_1, d_2, d_3 are pure imaginary. Set

$$C = \begin{bmatrix} I_{3\times3} & c_1D \\ -c_2D & I_{3\times3} \end{bmatrix},$$

we notice that

$$\begin{bmatrix} I_{3\times3} & -c_1D \\ c_2D & I_{3\times3} \end{bmatrix} = -C + 2I_{6\times6}.$$

Therefore, the magnitude matrix

$$G = C^{-1}(-C + 2I_{6\times6}) = -I_{6\times6} + 2C^{-1}.$$

Since D has three different eigenvalues

$$\lambda_1^D = 0, \qquad \lambda_{2,3}^D = \pm\sqrt{|d_1|^2 + |d_2|^2 + |d_3|^2},$$

there exists a matrix P such that

$$D = P \wedge P^{-1},$$

where

$$\wedge = \begin{bmatrix} \lambda_1^D & & \\ & \lambda_2^D & \\ & & \lambda_3^D \end{bmatrix}.$$

Thus we have

$$\lambda I_{6\times 6} - C = \begin{bmatrix} (\lambda-1)I_{3\times 3} & -c_1 D \\ c_2 D & (\lambda-1)I_{3\times 3} \end{bmatrix} = \begin{bmatrix} P & \\ & P \end{bmatrix} \begin{bmatrix} (\lambda-1)I_{3\times 3} & -c_1\wedge \\ c_2\wedge & (\lambda-1)I_{3\times 3} \end{bmatrix} \begin{bmatrix} P^{-1} & \\ & P^{-1} \end{bmatrix}. \tag{3.3}$$

From

$$|\lambda I_{6\times 6} - C| = \begin{vmatrix} (\lambda-1)I_{3\times 3} & -c_1\wedge \\ c_2\wedge & (\lambda-1)I_{3\times 3} \end{vmatrix} = 0,$$

it is easy to verify that the matrix C has eigenvalues

$$\lambda^C = 1 \pm i\sqrt{c_1 c_2}\lambda^D.$$

Therefore, the eigenvalues of C are

$$\lambda^C_{1,2} = 1, \qquad \lambda^C_{3,4} = 1 + i\sqrt{c_1 c_2}\sqrt{|d_1|^2 + |d_2|^2 + |d_3|^2},$$
$$\lambda^C_{5,6} = 1 - i\sqrt{c_1 c_2}\sqrt{|d_1|^2 + |d_2|^2 + |d_3|^2}.$$

The relationship between λ^G (the eigenvalue of G) and λ^C (the eigenvalue of C) is

$$\lambda^G = -1 + \frac{2}{\lambda^C}.$$

Thus, the eigenvalues of G are

$$\lambda^G_{1,2} = 1, \qquad \lambda^G_{3,4} = \frac{1 - i\sqrt{c_1 c_2}\sqrt{|d_1|^2 + |d_2|^2 + |d_3|^2}}{1 + i\sqrt{c_1 c_2}\sqrt{|d_1|^2 + |d_2|^2 + |d_3|^2}},$$
$$\lambda^G_{5,6} = \frac{1 + i\sqrt{c_1 c_2}\sqrt{|d_1|^2 + |d_2|^2 + |d_3|^2}}{1 - i\sqrt{c_1 c_2}\sqrt{|d_1|^2 + |d_2|^2 + |d_3|^2}}.$$

So we have

$$|\lambda^G| \equiv 1.$$

Therefore, the MSWCM (2.10) is unconditionally stable, which ends the proof. □

Substituting a plane wave

$$\begin{bmatrix} \mathbf{E} \\ \mathbf{H} \end{bmatrix} = e^{(k_x x + k_y y + k_z z - \omega t)} \begin{bmatrix} \mathbf{E} \\ \mathbf{H} \end{bmatrix}^0,$$

into (2.1), we can obtain the following dispersive relations [21]

$$\omega_{1,2} = 0, \quad \omega_{3,4} = \sqrt{(k_x^2 + k_y^2 + k_z^2)/\varepsilon\mu}, \quad \omega_{5,6} = -\sqrt{(k_x^2 + k_y^2 + k_z^2)/\varepsilon\mu}. \tag{3.4}$$

Then, substituting a discrete wave solution

$$\begin{bmatrix} \mathbf{E}^n_{l,j,k} \\ \mathbf{H}^n_{l,j,k} \end{bmatrix} = \begin{bmatrix} \mathbf{E} \\ \mathbf{H} \end{bmatrix}^0 e^{i(k_x l h_x + k_y j h_y + k_z k h_z - \omega n \tau)},$$

into the MSWCM (2.10), we obtain the corresponding numerical dispersion relations

$$\omega_{1,2} = 0, \tag{3.5a}$$

$$\omega_{3,4} = \frac{\tan^{-1}(\tau\sqrt{(|d_1|^2+|d_2|^2+|d_3|^2)/\varepsilon\mu})}{\tau}, \tag{3.5b}$$

$$\omega_{5,6} = -\frac{\tan^{-1}(\tau\sqrt{(|d_1|^2+|d_2|^2+|d_3|^2)/\varepsilon\mu})}{\tau}. \tag{3.5c}$$

Suppose h_x, h_y, h_z and τ tends to zero, noticing that

$$\sum_{l=1}^{M-1} 2\theta'(l)l = 1 \quad \text{and} \quad 2^{J_x}h_x = 1,$$

we have

$$|d_1| = \left|2^{J_x}\sum_{l=1}^{M-1} 2\theta'(l)\sin(k_x l h_x)\right| \approx \left|2^{J_x}h_x \cdot k_x \cdot \sum_{l=1}^{M-1} 2\theta'(l)l\right| = |k_x|.$$

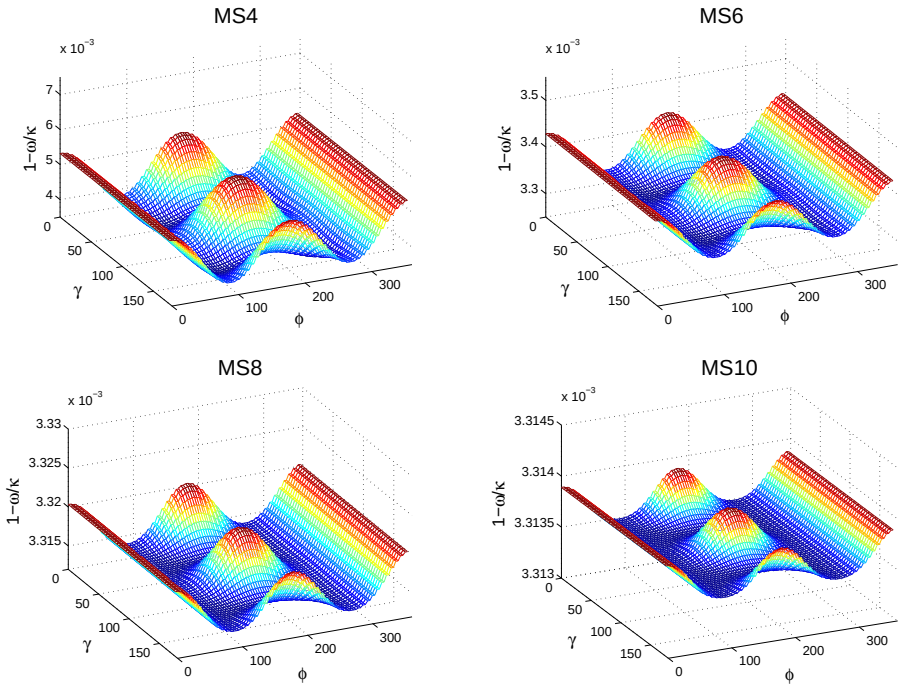

Figure 1: The numerical errors in phase velocity $\omega/\kappa - 1$ of $MS4$,$MS6$,$MS8$ and $MS10$ ($\tau = 0.1$, $h = 0.5$).

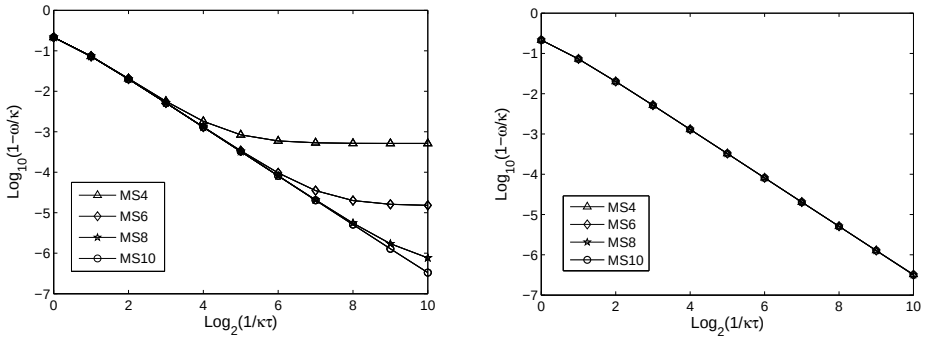

(a) (b)

Figure 2: Log-log plots for numerical phase velocity errors of MSM for the wave direction $\gamma = 45^\circ$ and $\phi = 90^\circ$, (a) $h = 2^{-1}$ (b) $h = 2^{-5}$.

Similarly, we have

$$|d_2| \approx |k_y| \quad \text{and} \quad |d_3| \approx |k_z|.$$

Therefore, the numerical dispersion relations in (3.5) converge to the continuous cases in (3.4) respectively.

Consider wave vector $\mathbf{k}$ in spherical coordinates

$$\begin{bmatrix} k_x \\ k_y \\ k_z \end{bmatrix} = \begin{bmatrix} \kappa \sin\gamma \cos\phi \\ \kappa \sin\gamma \sin\phi \\ \kappa \cos\gamma \end{bmatrix}, \qquad 0 \le \gamma \le 180^\circ, \qquad 0 \le \phi \le 360^\circ, \tag{3.6}$$

with

$$|\mathbf{k}| = \kappa = 1.$$

We choose $\tau = 0.1$ and $h_x = h_y = h_z = h = 0.5$, Fig. 1 shows the wave velocity $\omega/\kappa = \omega_3/\kappa$ for $MS4$, $MS6$, $MS8$ and $MS10$ across the full ranges of γ and ϕ, which illustrates that the numerical phase velocity errors of all methods MSM are very small. The log-log plots of $1 - \omega/\kappa$ vs. $1/(\kappa\tau)$ are shown in Fig. 2. we can see that the numerical phase velocity errors approach zero as τ and h approach zero.

Theorem 3.2. *Under periodic boundary conditions, the MSWCM* (2.10) *conserves the discrete total energy conservation laws* (2.5a) *and* (2.5b), *that is,*

$$\varepsilon\|\mathbf{E}^n\|^2 + \mu\|\mathbf{H}^n\|^2 = Constant, \tag{3.7a}$$

$$\varepsilon\|\delta_t\mathbf{E}^n\|^2 + \mu\|\delta_t\mathbf{H}^n\|^2 = Constant, \tag{3.7b}$$

where

$$\|\mathbf{E}^n\|^2 = h_x h_y h_z \sum_{l=1}^{N_x}\sum_{j=1}^{N_y}\sum_{k=1}^{N_z}\left((E_x{}^n_{l,j,k})^2 + (E_y{}^n_{l,j,k})^2 + (E_z{}^n_{l,j,k})^2\right),$$

$$\|\mathbf{H}^n\|^2 = h_x h_y h_z \sum_{l=1}^{N_x}\sum_{j=1}^{N_y}\sum_{k=1}^{N_z}\left((H_x{}^n_{l,j,k})^2 + (H_y{}^n_{l,j,k})^2 + (H_z{}^n_{l,j,k})^2\right).$$

Proof. We make inner product for the six equations of (2.10) with $\varepsilon\mathbf{E_x}^{n+1/2}$, $\varepsilon\mathbf{E_y}^{n+1/2}$, $\varepsilon\mathbf{E_z}^{n+1/2}$, $\mu\mathbf{H_x}^{n+1/2}$, $\mu\mathbf{H_y}^{n+1/2}$ and $\mu\mathbf{H_z}^{n+1/2}$ respectively, it yields

$$\begin{cases} \varepsilon\dfrac{\langle\mathbf{E_x}^{n+1},\mathbf{E_x}^{n+1}\rangle-\langle\mathbf{E_x}^{n},\mathbf{E_x}^{n}\rangle}{2\tau}=\langle(A_2\mathbf{H_z}^{n+\frac{1}{2}}-A_3\mathbf{H_y}^{n+\frac{1}{2}}),\mathbf{E_x}^{n+\frac{1}{2}}\rangle,\\ \varepsilon\dfrac{\langle\mathbf{E_y}^{n+1},\mathbf{E_y}^{n+1}\rangle-\langle\mathbf{E_y}^{n},\mathbf{E_y}^{n}\rangle}{2\tau}=\langle(A_3\mathbf{H_x}^{n+\frac{1}{2}}-A_1\mathbf{H_z}^{n+\frac{1}{2}}),\mathbf{E_y}^{n+\frac{1}{2}}\rangle,\\ \varepsilon\dfrac{\langle\mathbf{E_z}^{n+1},\mathbf{E_z}^{n+1}\rangle-\langle\mathbf{E_z}^{n},\mathbf{E_z}^{n}\rangle}{2\tau}=\langle(A_1\mathbf{H_y}^{n+\frac{1}{2}}-A_2\mathbf{H_x}^{n+\frac{1}{2}}),\mathbf{E_z}^{n+\frac{1}{2}}\rangle,\\ \mu\dfrac{\langle\mathbf{H_x}^{n+1},\mathbf{H_x}^{n+1}\rangle-\langle\mathbf{H_x}^{n},\mathbf{H_x}^{n}\rangle}{2\tau}=-\langle(A_2\mathbf{E_z}^{n+\frac{1}{2}}-A_3\mathbf{E_y}^{n+\frac{1}{2}}),\mathbf{H_x}^{n+\frac{1}{2}}\rangle,\\ \mu\dfrac{\langle\mathbf{H_y}^{n+1},\mathbf{H_y}^{n+1}\rangle-\langle\mathbf{H_y}^{n},\mathbf{H_y}^{n}\rangle}{2\tau}=-\langle(A_3\mathbf{E_x}^{n+\frac{1}{2}}-A_1\mathbf{E_z}^{n+\frac{1}{2}}),\mathbf{H_y}^{n+\frac{1}{2}}\rangle,\\ \mu\dfrac{\langle\mathbf{H_z}^{n+1},\mathbf{H_z}^{n+1}\rangle-\langle\mathbf{H_z}^{n},\mathbf{H_z}^{n}\rangle}{2\tau}=-\langle(A_1\mathbf{E_y}^{n+\frac{1}{2}}-A_2\mathbf{E_x}^{n+\frac{1}{2}}),\mathbf{H_z}^{n+\frac{1}{2}}\rangle. \end{cases} \tag{3.8}$$

In addition, since A_1, A_2, A_3 are anti-symmetric matrices, they satisfy the following formula

$$\langle A_i\mathbf{u},\mathbf{v}\rangle+\langle A_i\mathbf{v},\mathbf{u}\rangle=0,\quad \forall\mathbf{u},\mathbf{v}\in\mathbb{R}^{N_xN_yN_z},\quad i=1,2,3.$$

Then, we can sum all terms in the Eq. (3.8) and it is easily observed that the right hand side is offset. Thus, we obtain

$$\frac{1}{2\tau}\Big\{\big(\varepsilon\|\mathbf{E}^{n+1}\|^2+\mu\|\mathbf{H}^{n+1}\|^2\big)-\big(\varepsilon\|\mathbf{E}^{n}\|^2+\mu\|\mathbf{H}^{n}\|^2\big)\Big\}=0,$$

which leads to the first energy conservation law (3.7a).

Define a difference operator

$$\delta_t\omega^{n+\frac{1}{2}}=(\omega^{n+1}-\omega^n)\tau^{-1}.$$

Acting the operator δ_t on each terms of (2.10), then making inner products for the resulting equations with $\varepsilon\delta_t\mathbf{E_x}^{n+1/2}$, $\varepsilon\delta_t\mathbf{E_y}^{n+1/2}$, $\varepsilon\delta_t\mathbf{E_z}^{n+1/2}$, $\mu\delta_t\mathbf{H_x}^{n+1/2}$, $\mu\delta_t\mathbf{H_y}^{n+1/2}$ and $\mu\delta_t\mathbf{H_z}^{n+1/2}$ respectively, following the proof of the first energy conservation law (3.7a), we obtain the second energy conservation law (3.7b). □

4 ES-SWCM for the 3-D Maxwell's equations

In this section, we first discuss the properties of the wavelet spectral matrix in detail and make comparisons with Fourier spectral matrix, then we construct ES-SWCM for the 3-D Maxwell's equations.

4.1 The properties of the wavelet spectral matrix

Using Fourier transformation, the kth order differentiation matrix B_k of wavelet collocation method can be transformed to a diagonal form [23]

$$diag\big(\theta_1^{(k)},\theta_2^{(k)},\cdots,\theta_N^{(k)}\big)=\Theta^k,$$

where

$$\theta_l^{(k)} = 2^J \widetilde{\theta}^{(k)}(\omega_l), \quad l = 1, 2, \cdots, N,$$

are the eigenvalues of the matrix B_k. Here

$$\omega_l = -\frac{2\pi}{N}(l-1),$$

J is the scale, $\widetilde{\theta}^{(k)}(\omega)$ is the Fourier transform of $\theta^{(k)}(x)$. We call Θ^k as the kth order wavelet spectral matrix and note that

$$\Theta^k = diag\big(\lambda_0, \lambda_1, \cdots, \lambda_{\frac{N}{2}-1}, \lambda_{\frac{N}{2}}, \lambda_{\frac{N}{2}+1}, \cdots, \lambda_{N-1}\big).$$

The properties of Θ^k are presented in the following theorem.

Theorem 4.1. *The wavelet spectral matrix Θ^k has the following properties*

(1) $\lambda_{N-j} = \overline{\lambda_j}$, $j = 1, 2, \cdots, \frac{N}{2}$;

(2) when $k = 2m+1$, $\lambda_0 = \lambda_{\frac{N}{2}} = 0$; $\lambda_{N-j} = -\lambda_j$, $j = 1, 2, \cdots, \frac{N}{2} - 1$. λ_j *is pure imaginary;*

(3) when $k = 4m+2$, $\lambda_0 = 0$, $\lambda_{\frac{N}{2}} < 0$; $\lambda_{N-j} = \lambda_j$, $j = 1, 2, \cdots, \frac{N}{2} - 1$, λ_j *is real and* $\lambda_j < 0$;

(4) when $k = 4m$, $\lambda_0 = 0$, $\lambda_{\frac{N}{2}} > 0$; $\lambda_{N-j} = \lambda_j$, $j = 1, 2, \cdots, \frac{N}{2} - 1$, λ_j *is real and* $\lambda_j > 0$.

Proof. For part (1), since

$$\lambda_j = \sum_{r=-(M-1)}^{M-1} \theta^{(k)}(r) e^{ir\cdot(-j\frac{2\pi}{N})},$$

we have

$$\lambda_{N-j} = \sum_{r=-(M-1)}^{M-1} \theta^{(k)}(r) e^{ir(-(N-j)\frac{2\pi}{N})} = \sum_{r=-(M-1)}^{M-1} \theta^{(k)}(r) e^{ir\cdot(j\frac{2\pi}{N})} = \overline{\lambda_j}. \tag{4.1}$$

For part (2), since

$$\theta^{(k)}(-r) = -\theta^{(k)}(r), \quad \text{for } k = 2m+1,$$

we have

$$\begin{aligned} \lambda_{\frac{N}{2}} &= \sum_{r=-(M-1)}^{M-1} \theta^{(k)}(r) e^{ir(-\frac{N}{2}\frac{2\pi}{N})} = \sum_{r=-(M-1)}^{M-1} \theta^{(k)}(r)(-1)^{|r|} \\ &= \sum_{r=-(M-1)}^{M-1} \theta^{(k)}(r) = \lambda_0 = 0. \end{aligned} \tag{4.2}$$

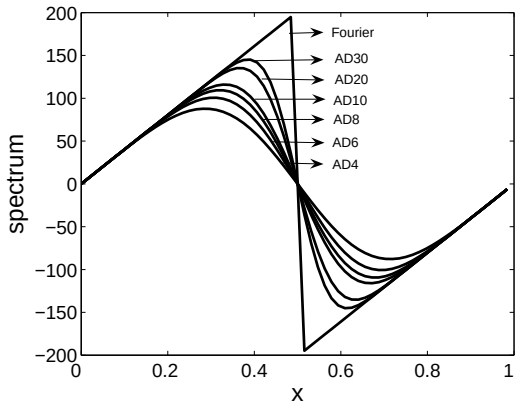

Figure 3: Elements of the wavelet spectral matrix with different ADM and the Fourier spectral matrix.

In addition, for $j = 1, 2, \cdots, N/2 - 1$, we have

$$\lambda_{N-j} = \overline{\lambda_j} = \sum_{r=-(M-1)}^{M-1} -\theta^{(k)}(-r)e^{ir\cdot(j\frac{2\pi}{N})} = \sum_{r=-(M-1)}^{M-1} -\theta^{(k)}(r)e^{-ir\cdot(j\frac{2\pi}{N})} = -\lambda_j. \quad (4.3)$$

Therefore, λ_j is pure imaginary. The parts (3) and (4) can be easily proved by combining (1) with the Theorem 3.1 (4) in [23]. □

We compare the one order wavelet spectral matrix Θ^1 with the Fourier spectral matrix Θ in [10], which has elements

$$\theta_{\frac{N}{2}+1} = 0, \quad \theta_l = i\frac{2\pi}{L}(l-1), \quad \text{for } l = 1, 2, \cdots, \frac{N}{2},$$

and

$$\theta_l = -\theta_{N-l+2}, \quad \text{for } l = \frac{N}{2} + 2, \cdots, N,$$

where L is the area length. The elements of Θ^1 and Θ are both pure imaginary. Consider computational area $[0, 1]$ and grid number $N = 64$, we show the imaginary part of the elements of Θ^1 and Θ in Fig. 3. We can see that the elements of the wavelet spectral matrix approach that of the Fourier spectral matrix with increasing the order M of ADM.

4.2 ES-SWCM for the Maxwell's equations

Splitting scheme has been widely used in Hamiltonian system and has been successfully applied to solve Maxwell's equations [6,21,22]. We combine the splitting scheme with the wavelet spectral matrix to construct ES-SWCM for the 3-D Maxwell's equations. The Maxwell's equations can be split into two linear subproblems, each of which

amounts to three pairs of mutually uncoupled 1-D equations [21]

$$\left\{\begin{array}{l}\left\{\begin{array}{l}\dfrac{\partial E_x}{\partial t}=\dfrac{1}{\varepsilon}\dfrac{\partial}{\partial y}H_z,\\ \dfrac{\partial H_z}{\partial t}=\dfrac{1}{\mu}\dfrac{\partial}{\partial y}E_x,\end{array}\right.\\ \left\{\begin{array}{l}\dfrac{\partial E_y}{\partial t}=\dfrac{1}{\varepsilon}\dfrac{\partial}{\partial z}H_x,\\ \dfrac{\partial H_x}{\partial t}=\dfrac{1}{\mu}\dfrac{\partial}{\partial z}E_y,\end{array}\right.\\ \left\{\begin{array}{l}\dfrac{\partial E_z}{\partial t}=\dfrac{1}{\varepsilon}\dfrac{\partial}{\partial x}H_y,\\ \dfrac{\partial H_y}{\partial t}=\dfrac{1}{\mu}\dfrac{\partial}{\partial x}E_z,\end{array}\right.\end{array}\right. \qquad \left\{\begin{array}{l}\left\{\begin{array}{l}\dfrac{\partial E_x}{\partial t}=-\dfrac{1}{\varepsilon}\dfrac{\partial}{\partial z}H_y,\\ \dfrac{\partial H_y}{\partial t}=-\dfrac{1}{\mu}\dfrac{\partial}{\partial z}E_x,\end{array}\right.\\ \left\{\begin{array}{l}\dfrac{\partial E_y}{\partial t}=-\dfrac{1}{\varepsilon}\dfrac{\partial}{\partial x}H_z,\\ \dfrac{\partial H_z}{\partial t}=-\dfrac{1}{\mu}\dfrac{\partial}{\partial x}E_y,\end{array}\right.\\ \left\{\begin{array}{l}\dfrac{\partial E_z}{\partial t}=-\dfrac{1}{\varepsilon}\dfrac{\partial}{\partial y}H_x,\\ \dfrac{\partial H_x}{\partial t}=-\dfrac{1}{\mu}\dfrac{\partial}{\partial y}E_z,\end{array}\right.\end{array}\right. \tag{4.4}$$

or shorter

$$\frac{\partial z}{\partial t}=Az, \qquad \frac{\partial z}{\partial t}=Bz.$$

Each of the six pairs of the 1-D sub-system in (4.4) can be written as a generic case

$$\left\{\begin{array}{l}\dfrac{\partial u}{\partial t}=\alpha\dfrac{\partial v}{\partial y},\\ \dfrac{\partial v}{\partial t}=\beta\dfrac{\partial u}{\partial y}.\end{array}\right. \tag{4.5}$$

We convert the Eq. (4.5) to Fourier modes with wave numbers $\{\widetilde{u}_l\}_{l=1}^N$ and $\{\widetilde{v}_l\}_{l=1}^N$, which can be carried out by the FFTs in $\mathcal{O}(N^2\log_2 N)$ operations. Then we need to solve the following ODE:

$$\left\{\begin{array}{l}\dfrac{\partial \widetilde{u}_l}{\partial t}=\alpha\theta_l^{(1)}\widetilde{v}_l,\\ \dfrac{\partial \widetilde{v}_l}{\partial t}=\beta\theta_l^{(1)}\widetilde{u}_l,\end{array}\right. \tag{4.6}$$

which can be solved exactly and the solution is described in discrete Fourier space:

$$\left\{\begin{array}{l}\widetilde{u}_l^{n+1}=\cos\left(\overline{\theta}_l^{(1)}c\tau\right)\widetilde{u}_l^n+isgn(\alpha)\sqrt{\dfrac{\alpha}{\beta}}\sin\left(\overline{\theta}_l^{(1)}c\tau\right)\widetilde{v}_l^n,\\ \widetilde{v}_l^{n+1}=\cos\left(\overline{\theta}_l^{(1)}c\tau\right)\widetilde{v}_l^n+isgn(\beta)\sqrt{\dfrac{\beta}{\alpha}}\sin\left(\overline{\theta}_l^{(1)}c\tau\right)\widetilde{u}_l^n,\end{array}\right. \tag{4.7}$$

where $c=\sqrt{\alpha\beta}$ and $\overline{\theta}_l^{(1)}$ is the imaginary part of $\theta_l^{(1)}$, which is pure imaginary as proved in Theorem 4.1. Set

$$a=sgn(\alpha)\sqrt{\frac{\alpha}{\beta}}, \quad b=sgn(\beta)\sqrt{\frac{\beta}{\alpha}}, \quad s=\sin\left(\overline{\theta}_l^{(1)}c\tau\right) \quad \text{and} \quad d=\cos\left(\overline{\theta}_l^{(1)}c\tau\right),$$

the transform matrix can be written as

$$C = \begin{bmatrix} d & ias \\ ibs & d \end{bmatrix}.$$

It can be easily proved that

$$C^{\mathrm{T}} J C = J,$$

with

$$J = \begin{bmatrix} 0 & 1 \\ -1 & 0 \end{bmatrix},$$

so C is a symplectic matrix. Thus, the splitting wavelet collocation method for each 1-D sub-system is symplectic.

Then, we choose the second-order Strang splitting method

$$z(t+\tau) = e^{\frac{1}{2}A\tau} e^{B\tau} e^{\frac{1}{2}A\tau} z(t), \tag{4.8}$$

to compose the solutions of the subproblems and obtain an explicit splitting symplectic wavelet collocation method (ES-SWCM) for the Maxwell's equations. We briefly denote the ES-SWCM with ADM as ESM.

The two-dimensional Maxwell's equations for the TM polatization case (2.6) can be split into

$$\begin{cases} \dfrac{\partial E_z}{\partial t} = \dfrac{1}{\varepsilon}\dfrac{\partial}{\partial x} H_y, \\ \dfrac{\partial H_y}{\partial t} = \dfrac{1}{\mu}\dfrac{\partial}{\partial x} E_z, \end{cases} \qquad \begin{cases} \dfrac{\partial E_z}{\partial t} = -\dfrac{1}{\varepsilon}\dfrac{\partial}{\partial y} H_x, \\ \dfrac{\partial H_x}{\partial t} = -\dfrac{1}{\mu}\dfrac{\partial}{\partial y} E_z, \end{cases} \tag{4.9}$$

while the equations for two-dimensional TE polatization case (2.7) can be split into

$$\begin{cases} \dfrac{\partial E_x}{\partial t} = \dfrac{1}{\varepsilon}\dfrac{\partial}{\partial y} H_z, \\ \dfrac{\partial H_z}{\partial t} = \dfrac{1}{\mu}\dfrac{\partial}{\partial y} E_x, \end{cases} \qquad \begin{cases} \dfrac{\partial E_y}{\partial t} = -\dfrac{1}{\varepsilon}\dfrac{\partial}{\partial x} H_z, \\ \dfrac{\partial H_z}{\partial t} = -\dfrac{1}{\mu}\dfrac{\partial}{\partial x} E_y. \end{cases} \tag{4.10}$$

5 Numerical experiments

In this section, we simulate the 2-D and 3-D Maxwell's equations and investigate stability, accuracy and conservation properties of the proposed methods. The parameters are normalized to

$$\varepsilon = \mu = 1.$$

The autocorrelation function AD10 is used for the wavelet collocation methods in following examples except the comparison part in Example 5.1. Fixed-point iteration method with tolerance 10^{-15} is used in solving (2.10) and $\pi = 3.14159265358979323846$ is used. All the simulations are computed by a compiled code of Fortran 95 in the same machine.

5.1 Two-dimensional problem

Example 5.1. We show an accuracy test for the 2-D Maxwell's equations (2.6) with the following smooth solution

$$\begin{pmatrix} H_x \\ H_y \\ E_z \end{pmatrix} = \begin{pmatrix} -\beta \\ \alpha \\ 1 \end{pmatrix} \exp\big[\cos(\alpha x + \beta y + t)\big], \tag{5.1}$$

where

$$\alpha = \cos(0.3\pi) \quad \text{and} \quad \beta = \sin(0.3\pi).$$

The computational domain is $[0, 2\pi/\alpha] \times [0, 2\pi/\beta]$ with periodic boundary conditions. This problem is also considered in [7] which use discontinuous Hamiltonian finite element method (DHFEM).

First, we use MS10 and ES10 to solve the problem till time $t = 100$ for long time simulation. With different grid points, L^2 and L^∞ errors for H_x, H_y and E_z are presented in Table 1. As can be seen from the table, both methods have high accuracy and have computation costs to $\mathcal{O}(N^2)$. MS10 takes twice the CPU times of ES10. In addition, with different grid points and time-steps, Table 2 gives the maximum errors of energy I and II over the time interval $[0, 100]$ for MS10 and ES10. Fig. 4 shows the variation of the errors in the two energy conserved quantities of MS10 for the case $\tau = 0.001$ and $N_x = N_y = 32$. We can see that the conserved quantities are preserved exactly and the errors are independent of time-step and grid points. Moreover, compared with the DHFEM, the MSWCM and ES-SWCM also have high accuracy but can preserve energy conservation laws better.

Table 1: The numerical errors and CPU times of all methods ($\tau = 0.00001$, $t = 100$).

Mthd	$N_x \times N_y$	H_x		H_y		E_z		CPU (s)
		L^∞ error	L^2 error	L^∞ error	L^2 error	L^∞ error	L^2 error	
MS10	16×16	1.66E-02	9.64E-02	1.21E-02	7.00E-02	2.06E-02	1.19E-01	11266
	32×32	1.55E-04	5.85E-04	1.13E-04	4.25E-04	1.91E-04	7.23E-04	48136
	64×64	2.36E-07	7.72E-07	1.71E-07	5.61E-07	2.92E-07	9.54E-07	203245
ES10	16×16	1.66E-02	9.64E-02	1.21E-02	7.00E-02	2.06E-02	1.19E-01	6445
	32×32	1.55E-04	5.85E-04	1.13E-04	4.25E-04	1.91E-04	7.23E-04	26539
	64×64	2.34E-07	7.69E-07	1.70E-07	5.58E-07	2.89E-07	9.50E-07	107446

Table 2: The maximum errors in energy I and II over the time interval $[0, 100]$.

Mthd	$N_x \times N_y$	$\tau = 0.01$		$\tau = 0.001$		$\tau = 0.0001$	
		energy I	energy II	energy I	energy II	energy I	energy II
MS10	16×16	8.91E-11	5.81E-11	8.91E-11	6.92E-11	9.87E-11	2.60E-10
	32×32	1.46E-10	6.99E-11	1.45E-10	7.13E-11	1.48E-10	1.52E-10
	64×64	2.67E-10	1.06E-10	2.68E-10	1.07E-10	2.65E-10	1.46E-10
ES10	16×16	3.13E-12	4.58E-12	4.15E-12	6.08E-12	1.05E-11	6.42E-12
	32×32	4.15E-12	3.58E-11	5.00E-12	6.09E-11	1.10E-11	4.82E-11
	64×64	1.98E-11	4.63E-10	1.81E-11	6.61E-10	2.74E-11	4.97E-10

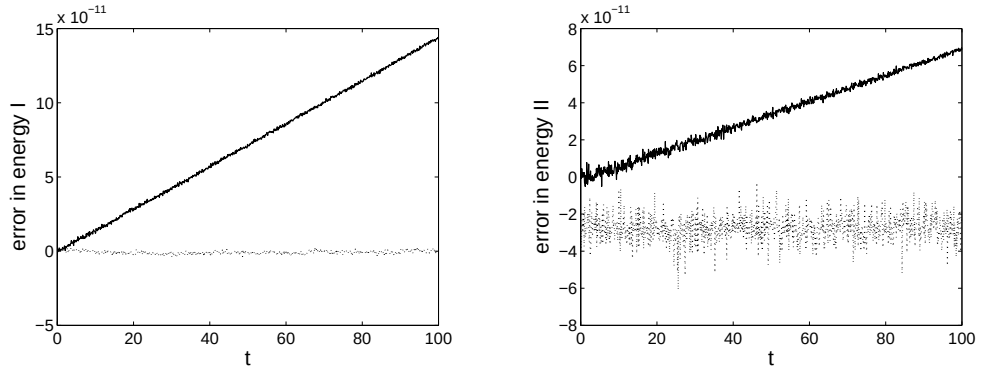

Figure 4: The variation of the errors in energy I and II of MS10 (-) and ES10 ($\cdot$) for the smooth solution (5.1), ($\tau = 0.001$, $N_x = N_y = 32$).

Second, we make a deep numerical investigation to show the tradeoff between computational effort and error for the MSWCM and the ES-SWCM. The numerical errors and CPU times are shown in Fig. 5. The first plot reveals that the numerical errors decrease when M or N becomes larger. The second plot shows that the ES-SWCM costs CPU times less than MS6, MS8 and MS10 but more than MS4. In the third plot, we can see that the connected line of the nods with the same grid points has a bigger slope than any of the four lines with the same M, which means that it is more efficient to increase M than N to obtain a smaller numerical error for this smooth solution.

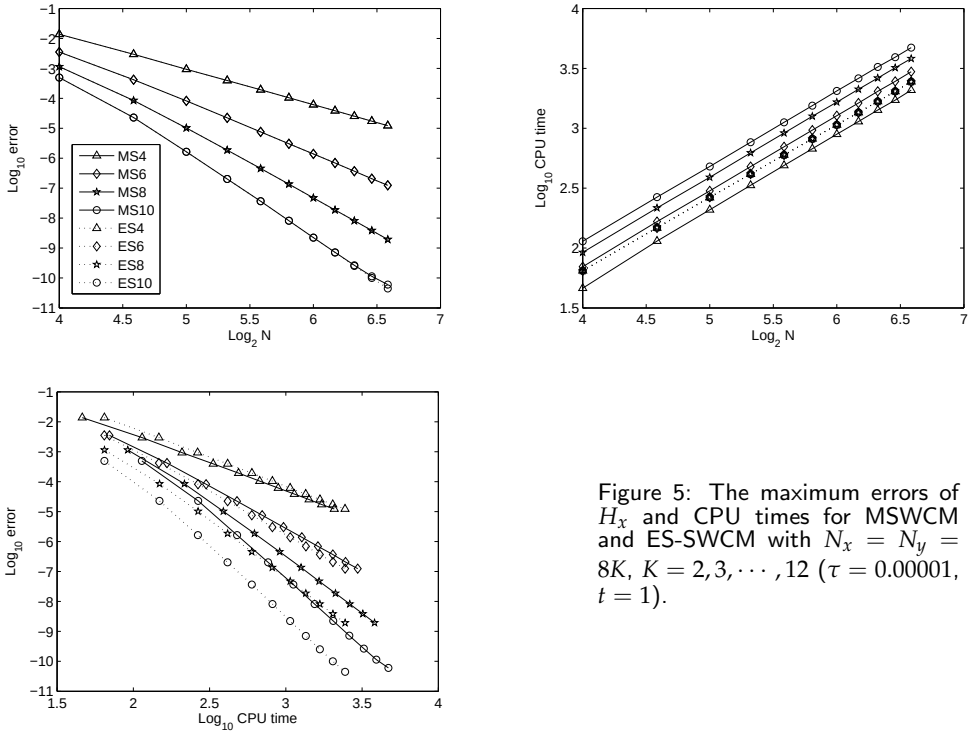

Figure 5: The maximum errors of H_x and CPU times for MSWCM and ES-SWCM with $N_x = N_y = 8K$, $K = 2, 3, \cdots, 12$ ($\tau = 0.00001$, $t = 1$).

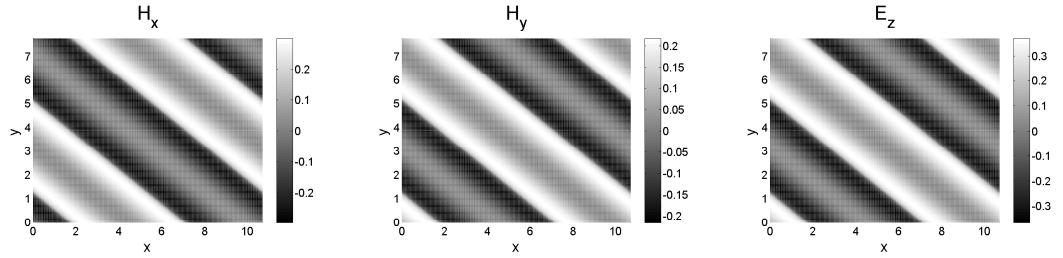

Figure 6: The contour plots for H_x, H_y, E_z of the non-smooth solution (5.2) at $t = 10$.

Example 5.2. Consider the following non-smooth solution of the 2-D Maxwell's equations (2.6) [7]

$$\begin{pmatrix} H_x \\ H_y \\ E_z \end{pmatrix} = \begin{pmatrix} -\beta \\ \alpha \\ 1 \end{pmatrix} \varphi\big(\cos(\alpha x + \beta y + t)\big), \tag{5.2}$$

where

$$\alpha = \cos(0.3\pi), \qquad \beta = \sin(0.3\pi),$$

$$\varphi(\omega) = \begin{cases} \omega \log(\omega), & \omega \neq 0, \\ 0, & \omega = 0. \end{cases} \tag{5.3}$$

Taking

$$\tau = 0.0002 \quad \text{and} \quad N_x = N_y = 320,$$

we use MS10 to solve the problem till time $t = 10$. We plot H_x, H_y and E_z at time $t = 10$ in Fig. 6. The L^∞ numerical errors for H_x, H_y and E_z are 9.39×10^{-3}, 6.82×10^{-3} and 1.16×10^{-2} respectively. The errors in the two energy conserved quantities are presented in Fig. 7. The results show that the MSWCM is stable, can capture singularity effectively and preserves the two energy conserved quantities very well.

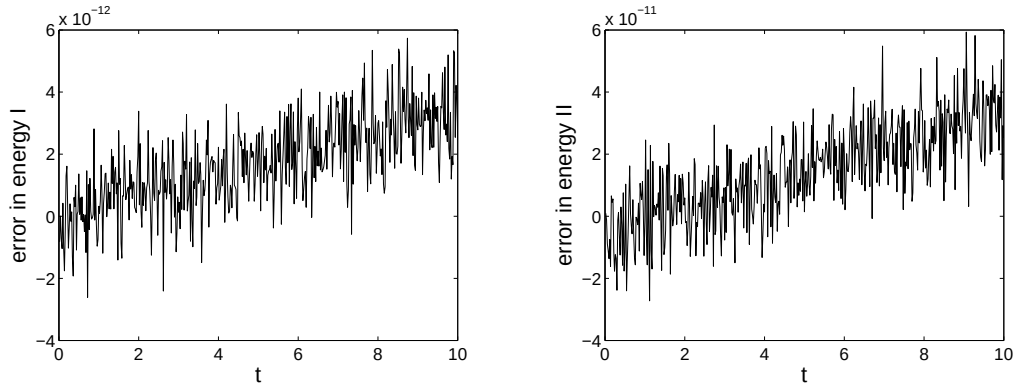

Figure 7: The variation of the errors in energy I and II of the non-smooth solution (5.2).

Example 5.3. Consider the following solution of the 2-D Maxwell's equations (2.7) (see [6])

$$E_x = \frac{k_y}{\varepsilon\sqrt{\mu}\omega}\cos(\omega\pi t)\cos(k_x\pi x)\sin(k_y\pi y), \tag{5.4a}$$

$$E_y = -\frac{k_x}{\varepsilon\sqrt{\mu}\omega}\cos(\omega\pi t)\sin(k_x\pi x)\cos(k_y\pi y), \tag{5.4b}$$

$$H_z = \frac{1}{\mu}\sin(\omega\pi t)\cos(k_x\pi x)\cos(k_y\pi y), \tag{5.4c}$$

where

$$\omega^2 = \frac{1}{\mu\varepsilon}(k_x^2 + k_y^2) \quad \text{and} \quad k_x = k_y = 10.$$

The computational domain is $[0,1]\times[0,1]$ with periodic boundary conditions. Taking $\tau = 0.0001$ and $N_x = N_y = 64$, we use MS10 to solve the problem till time $t = 10$. The numerical results with 16 contours for all components are shown in Fig. 8. The L^∞ numerical errors for E_x, E_y and H_z are 6.08×10^{-4}, 6.08×10^{-4} and 2.17×10^{-4} respectively. Errors in energy I and energy II are presented in Fig. 9. The two energy conserved quantities are preserved exactly. Compared with the results obtained by energy-conserved splitting FDTD methods (ECS-FDTD) in [6], the MSWCM can also preserve energy conservation laws very well but has higher accuracy.

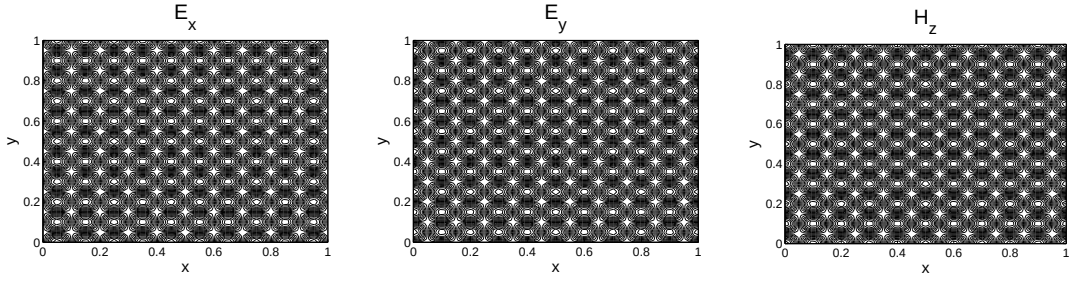

Figure 8: The contour plots for E_x, E_y, H_z of (2.7) with initial conditions (5.4) at $t = 10$.

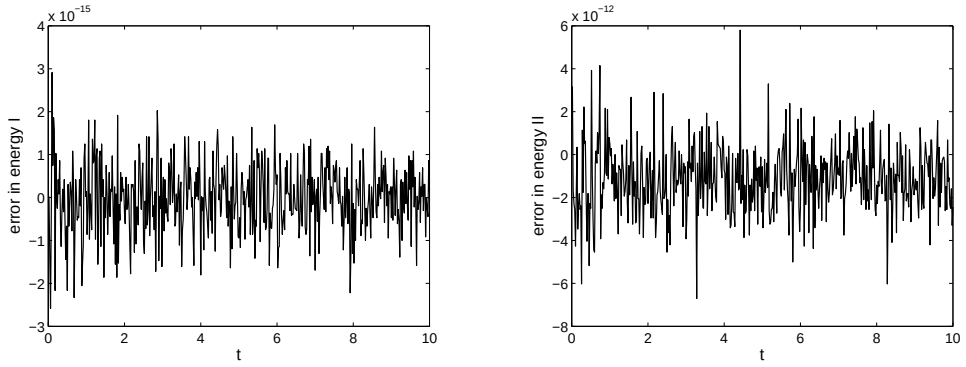

Figure 9: The variation of the errors in energy I and II.

5.2 Three-dimensional problem

Example 5.4. We consider the following periodic solution of the 3-D Maxwell's equations (2.2) [21,22]

$$\begin{cases} E_x = \cos\left(2\pi(x+y+z) - 2\sqrt{3}\pi t\right), & H_x = \sqrt{3}E_x, \\ E_y = -2E_x, & H_y = 0, \\ E_z = E_x, & H_z = -\sqrt{3}E_x. \end{cases} \tag{5.5}$$

The computational domain is $[0,1]\times[0,1]\times[0,1]$ with periodic boundary conditions.

First, taking the time-step $\tau = 0.0002$ and grid points $N_x = N_y = N_z = 32$, we use MS10 to solve the problem till time $t = 10$. Fig. 10 shows the L^2 and L^∞ numerical errors for all components, the numerical solution approximates the exact

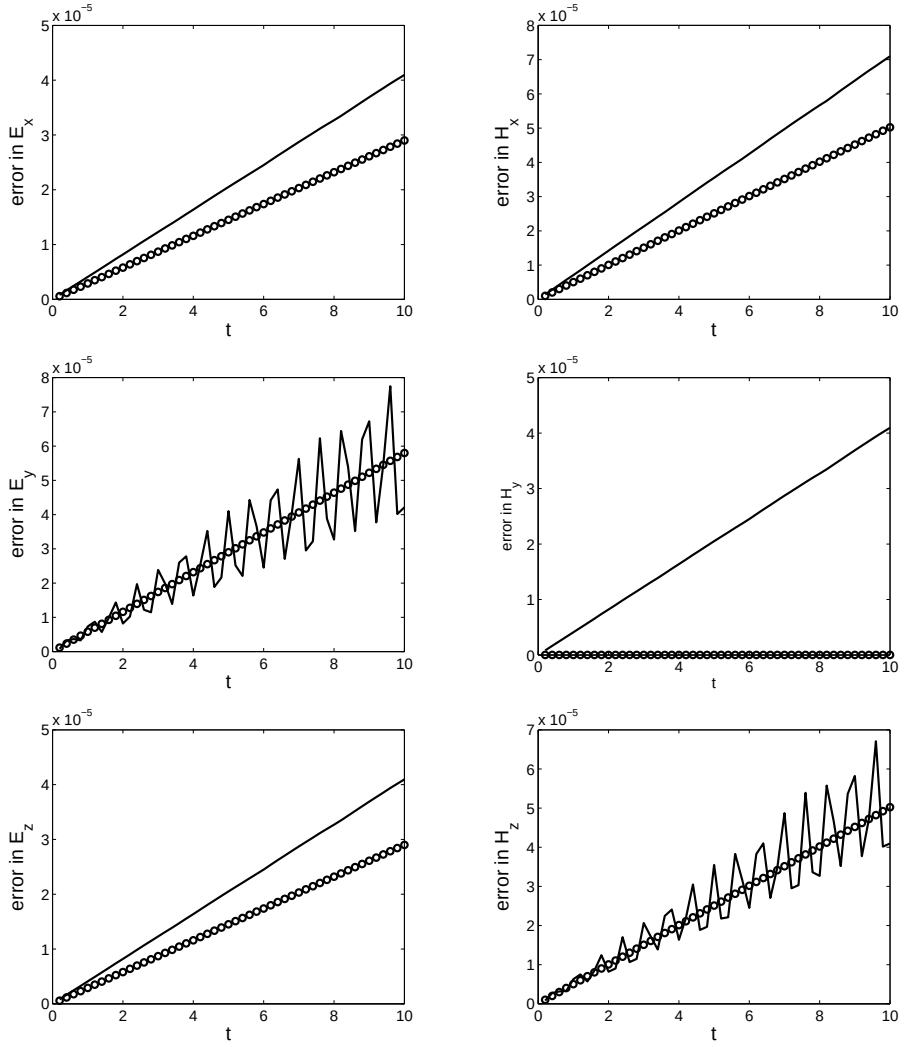

Figure 10: The numerical errors for all components in L_2 norm (o) and L_∞ norm (-) of the solution (5.5).

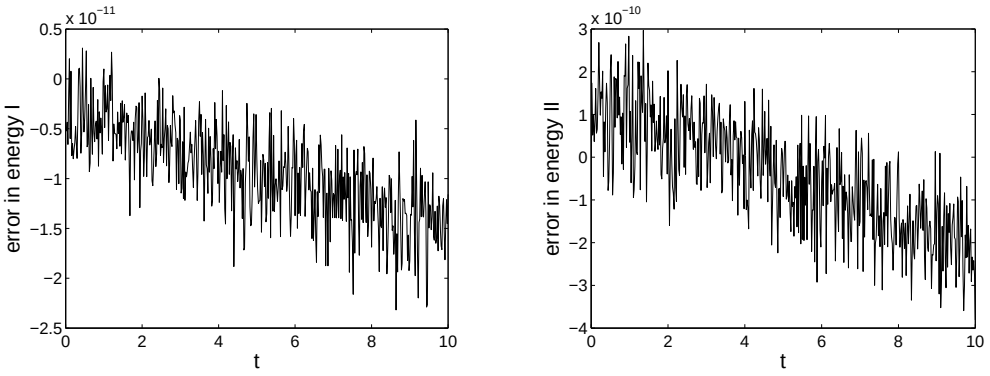

Figure 11: The variation of the error in energy I and II of the solution (5.5).

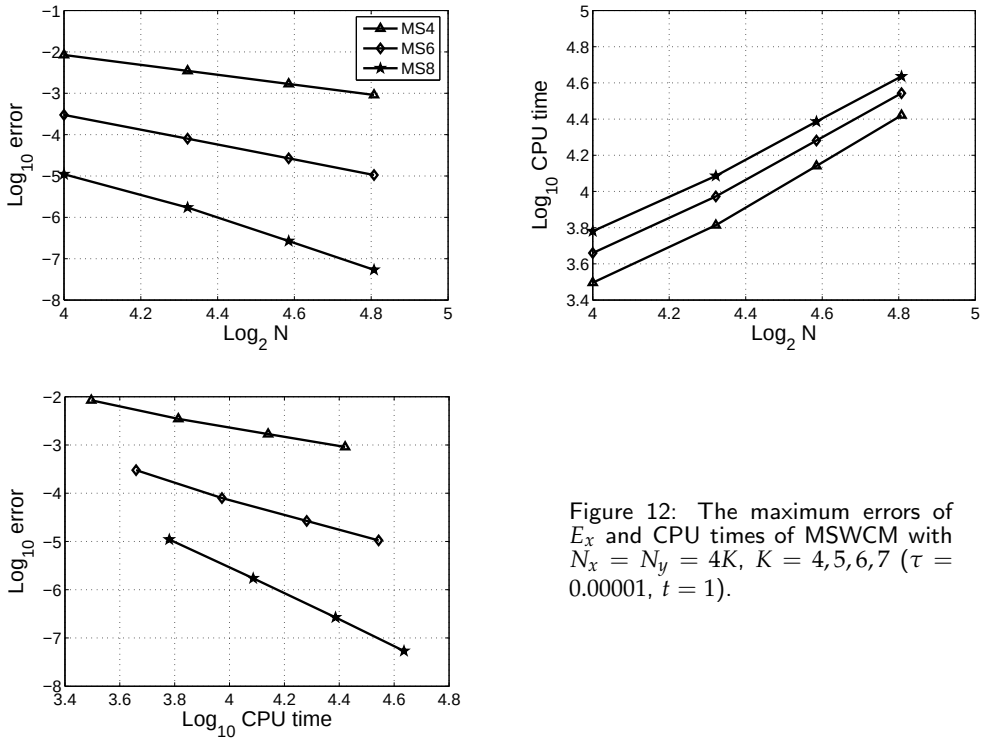

Figure 12: The maximum errors of E_x and CPU times of MSWCM with $N_x = N_y = 4K$, $K = 4,5,6,7$ ($\tau = 0.00001$, $t = 1$).

solution very well. Fig. 11 provides the errors in energy I and energy II, we can see that both energy I and energy II are preserved exactly. Compared with the results obtained by splitting multi-symplectic schemes (SMS) in [22], the MSWCM can also preserve the two energies very well but has higher spatial accuracy.

Second, we gives the numerical errors and CPU times of the MSWCM at $t = 1$ with different order M and grid number N in Fig. 12. Similarly with the 2-D case, it is more efficient to increase the order M than to increase grid number N for obtaining a smaller numerical error. The difference is that it costs CPU time near $\mathcal{O}(N^{\log_2 10})$ for the 3-D case which means the computational effort grows faster than the 2-D case

when the mesh is refined. However, we can see that a grid of $N_x = N_y = 32$ is enough to obtain a small numerical error, which shows the merits of the MSWCM having high accuracy.

Examples 5.1 and 5.2 reveal that the MSWCM has high accuracy similarly with the DHFEM but can preserve energy conservation laws better for both smooth and non-smooth case. Examples 5.3 and 5.4 reveal that the MSWCM can preserve the two energies exactly similarly with the ECS-FDTD and the SMS but has higher spatial accuracy. These results show that the MSWCM is an effective numerical method to simulate 2-D and 3-D Maxwell's equations with periodic boundary conditions.

6 Conclusions

Multi-symplectic wavelet collocation method is developed to solve Maxwell's equations. The spatial differentiation matrices of the MSWCM are sparse, which leads to less computation. The MSWCM has high spatial accuracy, can capture singularity efficiently and preserves energy conservation laws exactly during long time simulation. Compared with the ES-SWCM, the MSWCM has similar performance in accuracy and in preserving energy conservation laws. The results show that the MSWCM takes good balance of accuracy and efficiency and is an effective numerical method to simulate 2-D and 3-D Maxwell's equations with periodic boundary conditions. The MSWCM can be applied to solve the problem with mixed boundary conditions by introducing external wavelets near the boundary, and can be generalized to construct more structure preserving methods based on different wavelet basis. Moreover, the MSWCM can be naturally generalized to solve other multi-dimensional Hamiltonian PDEs.

Acknowledgments

This research was partially supported by the Natural Science Foundation of China (Grant No. 10971226 and No. 11001270) and the 973 Project of China (Grant No. 2009CB723802-4).

References

[1] K. S. YEE, *Numerical solution of initial boundary value problems involving Maxwell's equations in isotropic media*, IEEE T. Antenn. Propag., 14 (1966), pp. 302–307.

[2] M. KRUMPHOLZ AND L. P. B. KATEHI, *MRTD: new time-domain schemes based on multiresolution analysis*, IEEE T. Microw. Theory, 44 (1996), pp. 555–571.

[3] F. ZHENG, Z. CHEN AND J. ZHANG, *Toward the development of a three-dimensional unconditionally stable finite-difference time-domain method*, IEEE T. Microw. Theory, 48 (2000), pp. 1550–1558.

[4] L. GAO, B. ZHANG AND D. LIANG, *The splitting finite-difference time-domain methods for Maxwell's equations in two dimensions*, J. Comput. Appl. Math., 205 (2007), pp. 207–230.
[5] W. SHA, Z. X. HUANG, X. L. WU AND M. S. CHEN, *Application of the symplectic finite-difference time-domain scheme to electromagnetic simulation*, J. Comput. Phys., 225 (2007), pp. 33–50.
[6] W. B. CHEN, X. J. XI AND D. LIANG, *Energy-conserved splitting FDTD methods for Maxwell's equations*, Numer. Math., 108 (2008), pp. 445–485.
[7] Y. XU, JAAP J. W. VAN DER VEGT AND ONNO BOKHOVE, *Discontinuous Hamiltonian finite element method for linear hyperbolic systems*, J. Sci. Comput., 3 (2008), pp. 241–265.
[8] S. REICH, *Multi-symplectic Runge-Kutta collocation methods for Hamiltonian wave equations*, J. Comput. Phys., 157 (2000), pp. 473–499.
[9] T. J. BRIDGES AND S. REICH, *Multi-symplectic integrators: numerical schemes for Hamiltonian PDEs that conserve symplecticity*, Phys. Lett. A, 284 (2001), pp. 184–193.
[10] T. J. BRIDGES AND S. REICH, *Multi-symplectic spectral discretizations for the Zakharov-Kuznetsov and shallow water equations*, Phys. D, 152-153 (2001), pp. 491–504.
[11] E. HAIRER, CH. LUBICH AND G. WANNER, Geometric Numerical Integration: Structure-Preserving Algorithms for Ordinary Differential Equations, Springer, Berlin, 2002.
[12] A. L. ISLAS AND C. M. SCHOBER, *On the preservation of phase structure under multisymplectic discretization*, J. Comput. Phys., 197 (2004), pp. 585–609.
[13] B. E. MOORE AND S. REICH, *Multi-symplectic integrators for Hamiltonian PDEs*, Future Gener. Comp. Sy., 19 (2003), pp. 395–402.
[14] U. M. ASHER AND R. I. MCLACHLAN, *Multisymplectic box schemes and the Korteweg-de Vries equation*, Appl. Numer. Math., 48 (2004), pp. 255–269.
[15] J. L. HONG AND C. LI, *Multi-symplectic Runge-Kutta methods for nonlinear Dirac equations*, J. Comput. Phys., 211 (2006), pp. 448–472.
[16] J. L. HONG, S. S. JIANG, C. LI AND H. Y. LIU, *Explicit multisymplectic methods for Hamiltonian wave equations*, Commun. Comput. Phys., 2 (2007), pp. 662–683.
[17] J. L. HONG AND L. H. KONG, *Novel multi-symplectic integrators for nonlinear fourth-order Schrödinger equation with trapped term*, Commun. Comput. Phys., 7 (2010), pp. 613–630.
[18] J. B. CHEN, *Symplectic and multisymplectic Fourier pseudospectral discretizations for the Klein-Gordon equation*, Lett. Math. Phys., 75 (2006), pp. 293–305.
[19] Y. M. CHEN, H. J. ZHU AND S. H. SONG, *Multi-symplectic splitting method for the coupled nonlinear Schrödinger equation*, Comput. Phys. Commun., 181 (2010), pp. 1231–1241.
[20] J. X. CAI, Y. S. WANG, B. WANG AND B. JIANG, *New multisymplectic self-adjoint scheme and its composition scheme for the time-domain Maxwell's equations*, J. Math. Phys., 47 (2006), 123508.
[21] J. LEE AND B. FORNBERG, *A split step approach for the 3-D Maxwell's equations*, J. Comput. Appl. Math., 158 (2003), pp. 485–505.
[22] L. H. KONG, J. L. HONG AND J. J. ZHANG, *Splitting multisymplectic integrators for Maxwell's equations*, J. Comput. Phys., 229 (2010), pp. 4259–4278.
[23] H. J. ZHU, L. Y. TANG, S. H. SONG, Y. F. TANG AND D. S. WANG, *Symplectic wavelet collocation method for Hamiltonian wave equations*, J. Comput. Phys., 229 (2010), pp. 2550–2572.
[24] H. J. ZHU, S. H. SONG AND Y. F. TANG, *Multi-symplectic wavelet collocation method for the nonlinear Schrödinger and Camassa-Holm equations*, Comput. Phys. Commun., 182 (2010), pp. 616–627.
[25] H. J. ZHU, Y. M. CHEN, S. H. SONG AND H. Y. HU, *Symplectic and multi-symplectic wavelet collocation methods for two-dimensional Schrödinger equations*, Appl. Numer. Math.,

61 (2010), pp. 308–321.
[26] G. BEYLKIN, *On the representation of operators in bases of compactly supported wavelets*, SIAM J. Numer. Anal., 6 (1992), pp. 1716–1740.
[27] S. BERTOLUZZA AND G. NALDI, *A wavelet collocation method for the numerical solution of partial differential equations*, Appl. Comput. Harm. Anal., 3 (1996), pp. 1–9.
[28] O. V. VASILYEV AND S. PAOLUCCI, *A fast adaptive wavelet collocation algorithm for multidimensional PDEs*, J. Comput. Phys., 138 (1997), pp. 16–56.